Berry phase and topology in ultrastrongly coupled quantum light-matter systems

Kanta Masuki[1,*] and Yuto Ashida[1,2,†]

[1]*Department of Physics, University of Tokyo, 7-3-1 Hongo, Bunkyo-ku, Tokyo 113-0033, Japan*
[2]*Institute for Physics of Intelligence, University of Tokyo, 7-3-1 Hongo, Bunkyo-ku, Tokyo 113-0033, Japan*

Strong coupling between matter and quantized electromagnetic fields in a cavity has emerged as a possible route toward controlling the phase of matter in the absence of an external drive. We develop a faithful and efficient theoretical framework to analyze quantum geometry and topology in materials ultrastrongly coupled to cavity electromagnetic fields in two dimensions. The formalism allows us to accurately evaluate geometrical and topological quantities, such as Berry phase and Chern number, in ultrastrong and deep strong-coupling regimes. We apply our general framework to analyze a concrete model of massive Dirac fermions coupled to a circularly polarized cavity mode. Surprisingly, in addition to an ordinary transition to the topological phase, our analysis reveals a unique feature in deep strong-coupling regimes, namely the emergence of a reentrant transition to the topologically trivial phase. We also demonstrate its intuitive understanding by showing the unitary mapping between the low-energy effective theory of strongly coupled light-matter systems and the Haldane honeycomb model.

I. INTRODUCTION

The Berry phase plays a central role in modern condensed-matter physics [1–3]. It lies at the heart of a wide variety of intriguing phenomena, including electric polarization of crystalline insulators [3,4], the anomalous Hall effect [5–9], and electromagnetic responses [10–14]. In particular, the past few decades have witnessed significant advances in our understanding of the intimate connection between the Berry phase and topological phases of matter [15–23]. In addition, ongoing experimental developments in ultracold atoms [24–32] and photonics [33–40] have allowed us to study these rich phenomena in a highly controllable way.

On another front, recent developments have made it possible to realize strong interactions between matter and quantized electromagnetic fields inside a cavity [41–52]. In particular, the emergent field of cavity quantum electrodynamics (QED) materials has attracted significant attention as a possible platform for controlling the phase of matter in the absence of an external drive [53–57]. So far, the effects of cavity confinement on chemical reactions [58–72] and such diverse phenomena as superconductivity [73–78], ferroelectricity [79–82], and the quantum Hall effect [83–87] have been experimentally and theoretically investigated [88–126].

To further explore the potential of cavity QED engineering, the time is ripe to examine how strong light-matter interactions can influence the quantum geometrical and topological properties of matter. While related problems were often addressed by resorting to simplified phenomenological descriptions, such as Peierls substitution or minimally coupled effective Hamiltonians, the validity of these conventional approaches becomes questionable [56] in ultrastrong coupling (USC) and deep strong coupling (DSC) regimes, which are within reach of recent experiments [41–52,87,90–92]. Thus, the lack of a faithful and efficient theoretical approach to study quantum geometry and topology in ultrastrongly coupled systems remains a major current issue.

The aim of this paper is to develop a theoretical framework to accurately analyze geometrical and topological properties of matter coupled to cavity electromagnetic fields. To this end, we start from a general single-electron Hamiltonian with a single cavity mode [see Eq. (1) below]. After employing the asymptotically decoupling (AD) unitary transformation, we derive an expression of Berry curvature [Eq. (12)] that allows for its efficient evaluation at arbitrary coupling strengths on the basis of a simple tight-binding description. Our formalism thus provides a faithful and efficient way to evaluate the Berry phase and related topological numbers in generic two-dimensional cavity QED materials.

To demonstrate the advantage of the present formalism, we apply it to a concrete model of massive Dirac fermions on a honeycomb lattice potential, which can exhibit a cavity-induced topological phase transition (TPT). Figure 1 shows the phase diagram determined by the Chern number C of the lowest electron-polariton band. In the absence of the light-matter interaction ($g = 0$), a nonzero on-site energy difference Δ breaks the inversion symmetry, leading to the gap opening at the Dirac points and the trivial phase with $C = 0$ (see also Fig. 2 below). As the coupling strength g is increased, the transition to the topological phase with $C = 1$ can occur due to the time-reversal-symmetry (TRS) breaking inherent to the circularly polarized cavity mode. Interestingly, when the coupling g is further increased, the system exhibits the topological-to-trivial reentrant behavior in DSC regimes $g/\omega_c \gtrsim 1$. We show

*masuki@g.ecc.u-tokyo.ac.jp
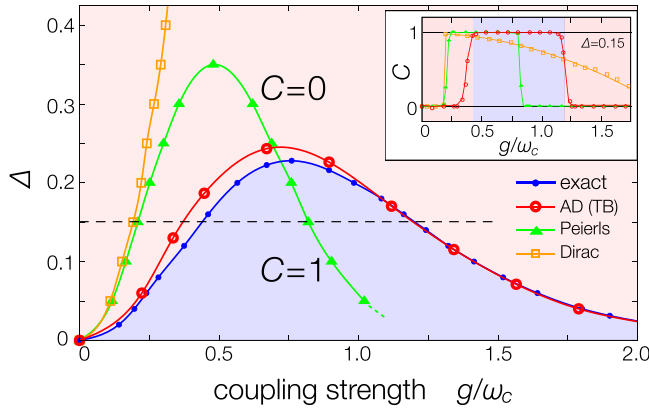†ashida@phys.s.u-tokyo.ac.jp

FIG. 1. Phase diagram of massive Dirac fermions coupled to circularly polarized cavity photons [cf. Eq. (1) with the honeycomb lattice potential (14)]. The phase boundary is determined by the Chern number C of the lowest electron-polariton band. At a small on-site energy difference Δ, the light-matter coupling g first gives rise to a transition from the trivial phase ($C = 0$) to the topological phase ($C = 1$), and then exhibits the reentrant behavior in DSC regimes ($g/\omega_c > 1$). We compare the phase boundaries obtained from different methods, including the exact analysis of Eq. (8) (blue), the tight-binding model (11) constructed in the AD frame (red), the tight-binding model with Peierls substitution (green), and the minimally coupled Dirac Hamiltonian (orange). The inset shows the corresponding Chern numbers at $\Delta = 0.15$. We take the unit of $\hbar = q = a = 1$ throughout this paper. Parameters are $m = 5$, $\omega_c = 4$, $V_0 = 1.5$.

that this nonmonotonic behavior can be understood from the connection between the low-energy effective theory of the present light-matter Hamiltonian and the Haldane honeycomb model [18].

The rest of the paper is organized as follows. In Sec. II, we start from the cavity QED Hamiltonian in the Coulomb gauge and construct the effective model in the AD frame. Then, in Sec. III, we provide the exact expression of Berry curvature in the AD frame (12) and its useful approximation. In Sec. IV, we apply our formalism to a concrete model of Dirac electrons coupled to a circularly polarized cavity mode, and we discuss the topological phase transitions in this system. We also perform thorough comparative analyses of geometrical and topological quantities, demonstrating the reliability of our approach compared to the commonly used methods in the literature (see Figs. 3 and 4). Section V summarizes the results and discusses the qualitative understandings of the topological phase transitions. Some technical details are discussed in the Appendixes.

II. MODEL DESCRIPTION

To illustrate our formalism in a simple yet experimentally relevant setup where Berry curvature can be nontrivial, we consider an electron interacting with a cavity mode in two dimensions, while the following discussions can be generalized to systems with multiple cavity modes in arbitrary dimensions. For the sake of simplicity, we neglect the electron spin degrees of freedom. We also assume that the photon loss is sufficiently small and consider the Hamiltonian under

the long-wavelength approximation, which is given in the Coulomb gauge as [127,128]

$$\hat{H}_C = \frac{(\hat{\boldsymbol{p}} - q\hat{\boldsymbol{A}})^2}{2m} + V(\boldsymbol{r}) + \hbar\omega_c\left(\hat{a}^\dagger\hat{a} + \frac{1}{2}\right), \quad (1)$$

$$\hat{\boldsymbol{A}} = A_0(\boldsymbol{f}\hat{a} + \boldsymbol{f}^*\hat{a}^\dagger), \quad \boldsymbol{f} \in \mathbb{C}^2. \quad (2)$$

Here, m and q are the mass and the charge of an electron, respectively, $V(\boldsymbol{r}) = \sum_{\boldsymbol{G}} V_{\boldsymbol{G}} e^{i\boldsymbol{G}\boldsymbol{r}}$ is an arbitrary two-dimensional periodic potential, and $\hat{a}^{(\dagger)}$ is the annihilation (creation) operator of cavity photons with frequency ω_c. An electron couples to cavity photons through the vector potential $\hat{\boldsymbol{A}}$ in Eq. (2), where A_0 is the mode amplitude, and $\boldsymbol{f}$ is an arbitrary polarization vector that satisfies $|\boldsymbol{f}| = 1$. The coupling strength of this light-matter interaction is characterized by

$$g = qA_0\sqrt{\frac{\omega_c}{m\hbar}}. \quad (3)$$

It is the common convention that the system is said to be in ultrastrong-coupling regimes for $0.1 \lesssim g/\omega_c \lesssim 1$ and deep strong-coupling regimes for $g/\omega_c \gtrsim 1$. We note that the cavity QED Hamiltonian (1) possesses TRS if and only if there exists $\theta \in \mathbb{R}$ such that the polarization vector $\boldsymbol{f}$ satisfies $\boldsymbol{f} = e^{i\theta}\boldsymbol{f}^*$. To examine the physically interesting case with broken TRS, we set $\boldsymbol{f}$ as a circularly polarized vector $\boldsymbol{e} = (1, -i)^T/\sqrt{2}$ in the following. See Appendixes A and B for the generalization to systems with arbitrary polarization or multiple electromagnetic modes. We expect that TRS-breaking cavity modes can be realized in chiral [54,55] or gyrotropic cavities [95,129].

The Hamiltonian (1) possesses the discrete translational symmetry of $V(\boldsymbol{r})$, which allows us to label its eigenstate as a Bloch state $|\psi_{n\boldsymbol{k}}^C\rangle$ with band index n and Bloch wave vector $\boldsymbol{k}$. In strong-coupling regimes, $|\psi_{n\boldsymbol{k}}^C\rangle$ is in general a highly entangled electron-photon state. A wide variety of experimental observables, including electromagnetic responses and transport coefficients, can be related to Berry curvature of these Bloch states:

$$B_n^C(\boldsymbol{k}) = i\left(\langle\partial_{k_x}u_{n\boldsymbol{k}}^C|\partial_{k_y}u_{n\boldsymbol{k}}^C\rangle - \langle\partial_{k_y}u_{n\boldsymbol{k}}^C|\partial_{k_x}u_{n\boldsymbol{k}}^C\rangle\right), \quad (4)$$

where $|u_{n\boldsymbol{k}}^C\rangle$ is the periodic part of the Bloch state defined by $|u_{n\boldsymbol{k}}^C\rangle = e^{-i\boldsymbol{k}\boldsymbol{r}}|\psi_{n\boldsymbol{k}}^C\rangle$. We again emphasize that $|u_{n\boldsymbol{k}}^C\rangle$ is not a mere electron state but an entangled wave function on the Hilbert space spanned by the product of electron and photon states.

In USC and DSC regimes, the calculation of Berry curvature (4) by the exact diagonalization of Eq. (1) becomes eventually intractable due to the need to include increasingly many electron-photon states in this frame. Instead, previous studies often resort to phenomenological descriptions such as Peierls substitution or minimally coupled effective Hamiltonians (see, e.g., Refs. [93,96,97]). However, as detailed below, these simplified methods become invalid at strong light-matter couplings. To accurately evaluate Berry curvature (4) and related topological numbers in an efficient way, we thus need to compress the dimension of the relevant Hilbert space while keeping nontrivial effects of light-matter interactions without making ambiguous simplifications.

To achieve this, we perform the AD transformation [98]

$$\hat{U} = \exp\left(-i\xi \frac{\hat{\boldsymbol{p}}}{\hbar} \cdot \hat{\boldsymbol{\pi}}\right), \qquad (5)$$

$$\xi = \sqrt{\frac{\hbar \omega_c}{m}} \frac{g}{\omega_c^2 + g^2}, \qquad (6)$$

$$\hat{\boldsymbol{\pi}} = -i e \hat{a} + i e^* \hat{a}^\dagger. \qquad (7)$$

The transformation $\hat{U}$ acts on the creation operator $\hat{a}^\dagger$ and the position operator $\boldsymbol{r}$ via $\hat{U}^\dagger \hat{a}^\dagger \hat{U} = \hat{a}^\dagger + \xi \hat{\boldsymbol{p}} \cdot \boldsymbol{e}/\hbar$ and $\hat{U}^\dagger \boldsymbol{r} \hat{U} = \boldsymbol{r} + \xi \hat{\boldsymbol{\pi}} + \xi^2 \hat{\boldsymbol{p}} \times \boldsymbol{e}_z/(2\hbar)$, respectively. We then obtain the transformed Hamiltonian $\hat{H}^U \equiv \hat{U}^\dagger \hat{H} \hat{U}$ as

$$\hat{H}^U = \frac{\hat{\boldsymbol{p}}^2}{2m_{\text{eff}}} + V\left(\boldsymbol{r} + \xi \hat{\boldsymbol{\pi}} + \frac{\xi^2}{2\hbar}\hat{\boldsymbol{p}} \times \boldsymbol{e}_z\right) + \hbar \Omega\left(\hat{a}^\dagger \hat{a} + \frac{1}{2}\right), \qquad (8)$$

$$m_{\text{eff}} = m\left(1 + \frac{g^2}{\omega_c^2}\right), \quad \Omega = \omega_c\left(1 + \frac{g^2}{\omega_c^2}\right). \qquad (9)$$

Here, m_{eff} is the effective mass dressed by cavity photons, and Ω is the renormalized cavity frequency due to the $\hat{\boldsymbol{A}}^2$-term in the Coulomb gauge (1). In this frame, the light-matter interaction is expressed as the shift of the electron coordinate $\boldsymbol{r}$, and its effective strength is characterized by the parameter ξ defined in Eq. (6). Because ξ behaves as $\xi \propto g$ at small g/ω_c and $\xi \propto g^{-1}$ at large g/ω_c, light and matter degrees of freedom are asymptotically decoupled in the weak- and strong-coupling limits. One can thus well approximate the low-energy eigenstates simply by the product state of an electron wave function and the photon vacuum $|0\rangle$. This feature allows us to construct a useful low-energy effective description in the following way.

First, we construct Wannier orbitals $|w_i\rangle$ from the matter part of $\hat{H}^U$:

$$\hat{H}^U_{\text{mat}} = \langle 0|\hat{H}^U|0\rangle = \frac{\hat{\boldsymbol{p}}^2}{2m_{\text{eff}}} + \sum_{\boldsymbol{G}} V_{\boldsymbol{G}} e^{-\frac{\xi^2 G^2}{4}} e^{i\boldsymbol{G} \cdot (\boldsymbol{r} + \frac{\xi^2}{2\hbar}\hat{\boldsymbol{p}} \times \boldsymbol{e}_z)}, \quad (10)$$

where $|0\rangle$ is the photon vacuum, and $V_{\boldsymbol{G}}$ is the Fourier component of the periodic potential $V(\boldsymbol{r})$ defined via $V(\boldsymbol{r}) = \sum_{\boldsymbol{G}} V_{\boldsymbol{G}} e^{-i\boldsymbol{G} \cdot \boldsymbol{r}}$. Secondly, we project the continuum Hamiltonian $\hat{H}^U$ onto the manifold spanned by these Wannier orbitals, obtaining the following tight-binding Hamiltonian:

$$\hat{H}^U_{\text{TB}} = \sum_{\langle ij \rangle} (t_{ij} + \hat{\mu}_{ij})|w_i\rangle\langle w_j|, \qquad (11)$$

where $t_{ij} = \langle w_i|\hat{H}^U_{\text{mat}}|w_j\rangle$ is an effective hopping amplitude, and $\hat{\mu}_{ij} = \langle w_i|(\hat{H}^U - \hat{H}^U_{\text{mat}})|w_j\rangle$ represents electromagnetic fluctuations.

In the newly obtained tight-binding Hamiltonian (11), the underlying Wannier orbitals $|w_i\rangle$ already incorporate light-matter interactions in a nonperturbative manner through the renormalized mass and potential in Eq. (10). The hopping amplitudes t_{ij} play the dominant role while the residual terms $\hat{\mu}_{ij}$ are typically negligible and do not qualitatively alter the results, as shown in Appendix D. We note that our construction of the tight-binding model makes a sharp contrast with usual phenomenological methods; for instance, in Peierls substitution, one starts from a tight-binding Hamiltonian $\sum_{\langle ij \rangle} t^0_{ij}|w^0_i\rangle\langle w^0_j|$ with the bare Wannier orbitals $|w^0_i\rangle$

in the absence of light-matter interactions and then replaces the hopping amplitudes t^0_{ij} by $t^0_{ij}\exp[i(q/\hbar)\int_{\boldsymbol{r}_j}^{\boldsymbol{r}_i} d\boldsymbol{r} \cdot \hat{\boldsymbol{A}}]$ with $\boldsymbol{r}_i = \langle w^0_i|\boldsymbol{r}|w^0_i\rangle$.

III. BERRY CURVATURE IN THE TRANSFORMED FRAME

We recall that physical observables can be related to Berry curvature (4), which is originally defined in the Coulomb gauge. To derive the exact expression of Berry curvature (4) after the unitary transformation, we note that the discrete translational symmetry remains intact in the transformed Hamiltonian (8), i.e., eigenstates in this frame are also Bloch states $|\psi^U_{n\boldsymbol{k}}\rangle = e^{i\boldsymbol{k}\boldsymbol{r}}|u^U_{n\boldsymbol{k}}\rangle$ and can be related to their Coulomb-gauge counterparts by $|u^U_{n\boldsymbol{k}}\rangle = \exp[\frac{i\xi}{\hbar}(\hat{\boldsymbol{p}} + \hbar\boldsymbol{k}) \cdot \hat{\boldsymbol{\pi}}]|u^C_{n\boldsymbol{k}}\rangle$. We can then rewrite Eq. (4) in terms of the transformed eigenstates as

$$B^C_n(\boldsymbol{k}) = i\left(\langle \partial_{k_x} u^U_{n\boldsymbol{k}}|\partial_{k_y} u^U_{n\boldsymbol{k}}\rangle - \langle \partial_{k_y} u^U_{n\boldsymbol{k}}|\partial_{k_x} u^U_{n\boldsymbol{k}}\rangle\right)$$
$$+ \xi\left[\nabla_{\boldsymbol{k}} \times \langle \psi^U_{n\boldsymbol{k}}|\hat{\boldsymbol{\pi}}|\psi^U_{n\boldsymbol{k}}\rangle\right]_{k_z} - \frac{\xi^2}{2\hbar}\nabla_{\boldsymbol{k}} \cdot \langle \psi^U_{n\boldsymbol{k}}|\hat{\boldsymbol{p}}|\psi^U_{n\boldsymbol{k}}\rangle, \qquad (12)$$

where the latter two terms originate from the $\boldsymbol{k}$-dependence of the unitary transformation between $|u^C_{n\boldsymbol{k}}\rangle$ and $|u^U_{n\boldsymbol{k}}\rangle$. See Appendix C for derivations.

The dominant contribution in Eq. (12) comes from the terms in the first line, while the other terms can be neglected due to the asymptote $\xi \propto g^{-1}$ at large g. Together with the fact that the electromagnetic fluctuations $\hat{\mu}_{ij}$ in Eq. (11) can also be neglected, the analysis of Berry phase in the transformed frame can be significantly simplified as follows:

$$B^C_n(\boldsymbol{k}) \simeq i\left(\langle \partial_{k_x} \tilde{u}^U_{n\boldsymbol{k}}|\partial_{k_y} \tilde{u}^U_{n\boldsymbol{k}}\rangle - \langle \partial_{k_y} \tilde{u}^U_{n\boldsymbol{k}}|\partial_{k_x} \tilde{u}^U_{n\boldsymbol{k}}\rangle\right), \qquad (13)$$

where $|\tilde{u}^U_{n\boldsymbol{k}}\rangle$ is an electron eigenstate of $\sum_{\langle ij \rangle} t_{ij}|w_i\rangle\langle w_j|$, which only contains the matter part of the tight-binding Hamiltonian (11). One can thus accurately and efficiently evaluate Berry curvature of ultrastrongly coupled systems simply by Eq. (13) without photon degrees of freedom. Instead, it is also possible to include higher-order terms to systematically improve quantitative accuracy when necessary. The same strategy is applicable to calculations of other geometric quantities such as Berry connection and quantum metric as described in Appendix C.

IV. HONEYCOMB MODEL

To be concrete, we consider a model of massive Dirac fermions on honeycomb lattice potential, that is, the light-matter Hamiltonian (1) with the following potential:

$$V(\boldsymbol{r}) = V_0\phi(\boldsymbol{r}) + \frac{\Delta}{9}\phi\left(\boldsymbol{r} - \frac{\boldsymbol{a}_1}{3} + \frac{\boldsymbol{a}_2}{3}\right), \qquad (14)$$

$$\phi(\boldsymbol{r}) = \sum_{\boldsymbol{G}=\pm\boldsymbol{b}_1, \pm\boldsymbol{b}_2, \pm(\boldsymbol{b}_1-\boldsymbol{b}_2)} \exp(i\boldsymbol{G} \cdot \boldsymbol{r}), \qquad (15)$$

where $\boldsymbol{a}_1 = (a, 0)$ and $\boldsymbol{a}_2 = (-a/2, \sqrt{3}a/2)$ are the primitive lattice vectors with their reciprocal counterparts $\boldsymbol{b}_1 = (2\pi/a, 2\pi/\sqrt{3}a)$ and $\boldsymbol{b}_2 = (0, 4\pi/\sqrt{3}a)$. As shown in Fig. 2(a), the minima of this potential are aligned on the
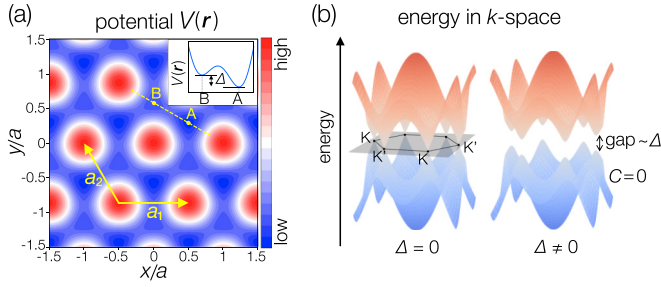
FIG. 2. (a) Honeycomb lattice potential $V(\mathbf{r})$ in Eq. (14). The inset shows the potential along the yellow dashed line, where Δ corresponds to the energy difference between the two sublattices. (b) Two lowest energy bands in the absence of cavity fields. Nonzero Δ opens an energy gap in the Dirac cones, where the lowest band is trivial with the Chern number $C = 0$.

FIG. 3. (a),(b) Absolute value of the Berry curvature of the lowest electron-polariton band at the Dirac point at different Δ in Eq. (14). We compare the results obtained from the exact Hamiltonian (8) with Eq. (F6), which is equivalent to Eq. (12) (blue), the electron-only tight-binding model with Eq. (13) (red), the tight-binding model with Peierls substitution (green), and the minimally coupled Dirac Hamiltonian (E4) (orange). Parameters are $m = 5$, $\omega_c = 4$, $V_0 = 1.5$, $\Delta = 0$.

honeycomb lattice, and the on-site energy difference between the two sublattices is given by Δ.

Figure 2(b) shows the two lowest energy bands in the absence of cavity electromagnetic fields. A nonzero Δ breaks the inversion symmetry and opens an energy gap $\sim \Delta$ in the Dirac cones [130], resulting in the topologically trivial lowest energy band with the Chern number $C = 0$. When the light-matter coupling is included, the TRS-breaking by the circularly polarized cavity mode is expected to trigger the eventual gap closing and the transition to the topologically nontrivial phase with $C = \pm 1$. While such a cavity-induced TPT was previously explored within a minimally coupled Dirac Hamiltonian [96,97], this simplified analysis can be justified only in perturbative regimes $g/\omega_c \ll 1$ as demonstrated below.

We now examine the low-energy properties of the present model on the basis of our formalism; hereafter we take the unit of $\hbar = q = a = 1$. To construct the effective tight-binding model (11), we use the maximally localized Wannier orbitals $|w_i\rangle$ of Eq. (10) [131–134] and consider up to the next-nearest-neighbor hoppings on the honeycomb lattice. We then analyze the behavior of Berry curvature, Chern number, and the corresponding energy spectrum with a varying coupling g, and we compare the results with the ones obtained from other methods. For instance, the results of a minimally coupled Dirac Hamiltonian are obtained with Eq. (E4). These results are compared to the exact results obtained by the exact diagonalization of the full continuum Hamiltonian (8) and using the exact expression of Berry curvature (F6), which is equivalent to Eq. (12). We note that the exact analyses in general require high computational costs, and it is crucial to develop an effective description to efficiently evaluate expectation values of physical observables as done here. See Appendixes E and F for further details.

Figure 1 shows the obtained phase diagram whose phase boundary is determined by the Chern number C of the lowest electron-polariton band, i.e., $C = (2\pi)^{-1} \int_{\mathrm{BZ}} d^2\mathbf{k} \, B_0^C(\mathbf{k})$. (As for the minimally coupled Dirac Hamiltonian, we determine the phase boundary by locating g at which the band gap closes.) At a small energy difference $\Delta \lesssim 0.2$, TPTs from the trivial phase ($C = 0$) to the topological phase ($C = 1$) can occur in USC regimes. Surprisingly, the system also exhibits
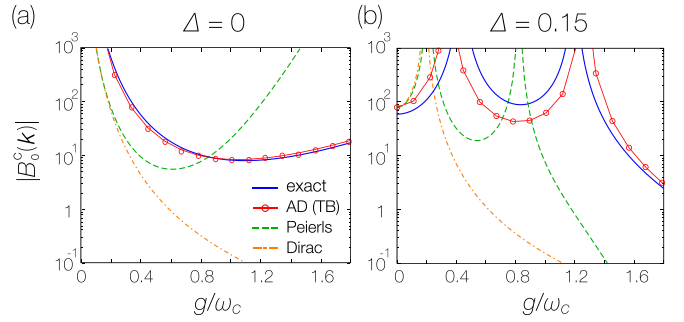
the reentrant transition to the trivial phase in DSC regimes $g/\omega_c \gtrsim 1$, whose interpretation will be given below. It is also worthwhile to emphasize that TPTs no longer exist at a sufficiently large Δ. The minimally coupled Dirac Hamiltonian (orange curve) fails to capture these intriguing features and, more importantly, it even gives an unquantized Chern number (see the inset). Peierls substitution also fails to give quantitatively accurate results once the USC regime $g/\omega_c \gtrsim 0.1$ is reached. In contrast, our tight-binding model (11) (red curve) remains valid over the whole parameter region at both qualitative and quantitative levels.

To make further comparisons, we plot the absolute value of the Berry curvature of the lowest electron-polariton band at the K-point, i.e., $\mathbf{k} = \mathbf{b}_1/3 + \mathbf{b}_2/3$, with a varying coupling g (Fig. 3). We note that the Berry curvature at the K-point takes a positive (negative) value in the topological (topologically trivial) phase. Again, our results (red curve) obtained from the formula (13) associated with the electron-only tight-binding model, $\sum_{\langle ij \rangle} t_{ij} |w_i\rangle \langle w_j|$, agree well with the exact results (blue curve) at arbitrary coupling strengths, while our results slightly deviate from the exact ones in the vicinity of the band-gap closing points [Fig. 3(b)]. Meanwhile, the other conventional descriptions dramatically fail in USC and DSC regimes, where Berry curvature is either under- or overestimated by orders of magnitude.

In Fig. 4, we also show the low-energy spectra at different coupling strengths. When the coupling g is increased, the Wannier orbitals in the AD frame become tightly localized around each potential minima due to the enhancement of the effective mass m_{eff} in Eq. (10). Thus, effective hopping amplitudes t_{ij} between different Wannier orbitals are exponentially suppressed, leading to the flattening of energy bands (blue and red curves). Peierls substitution (green curves) tends to overestimate this flattening behavior especially in DSC regimes. We note that the upward shift of the entire energy spectrum is caused by the increase of the zero-point energy $\hbar \Omega / 2$ of cavity photons with the renormalized frequency Ω, which cannot be captured by Peierls substitution. Similar behaviors can also be found at nonzero Δ.
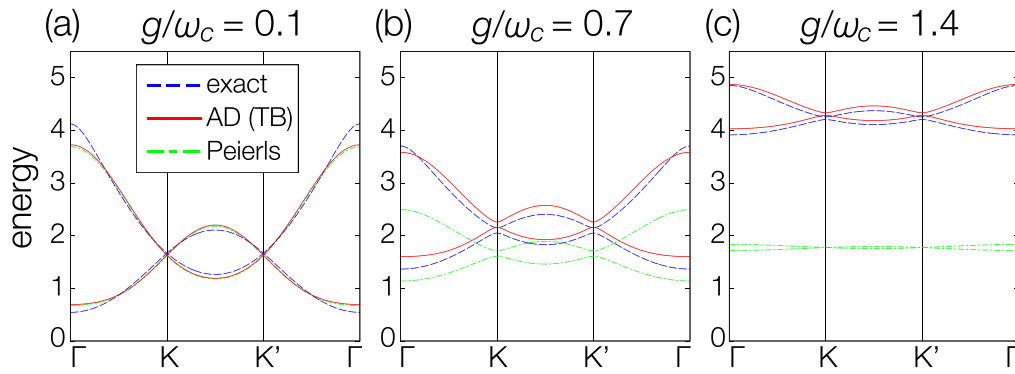
FIG. 4. Low-energy spectra at different coupling strengths obtained from the exact analysis of Eq. (8) (blue), the tight-binding model (11) in the AD frame (red), and the tight-binding model with Peierls substitution (green). K and K' denote the two Dirac points. Parameters are $m = 5$, $\omega_c = 4$, $V_0 = 1.5$, $\Delta = 0$.

We note that the minimally coupled Dirac Hamiltonian can be obtained by expanding the tight-binding Hamiltonian with Peierls substitutions around K and K' points. Thus, around these representative points, the low-energy spectrum evaluated from the minimally coupled Dirac Hamiltonian shows similar behaviors as in the result of the Peierls substitution as far as we consider a weak coupling $g/\omega_c \ll 1$. However, at large g, these two results disagree with each other, and, in particular, the minimally coupled Dirac Hamiltonian fails to reproduce the gap closing at the K-point, which corresponds to the reentrant topological phase transition shown in Fig. 1.

V. DISCUSSIONS AND CONCLUSIONS

We point out that our formalism reveals an intimate connection between quantum light-matter systems and the celebrated Haldane honeycomb model [18], which allows us to develop a simple understanding of the present results. To see this, we first recall that low-energy physics of the present light-matter systems can be well captured by the tight-binding Hamiltonian, $\sum_{\langle ij \rangle} t_{ij} |w_i\rangle\langle w_j|$, which only contains electron degrees of freedom. Here, as inferred from the TRS-breaking term $\xi^2 \boldsymbol{p} \times \boldsymbol{e}_z/(2\hbar)$ in Eq. (10), the effective hopping amplitudes t_{ij} are in general complex-valued. In particular, the next-nearest-neighbor hopping amplitudes t_2 in the present model acquire phase factors, and the resulting tight-binding Hamiltonian becomes equivalent to the Haldane honeycomb model. This analogy gives a simple interpretation of the reentrant TPT emerging in DSC regimes (Fig. 1). On the one hand, it is known in the Haldane model that reentrant transition to the trivial phase can occur when an imaginary part of t_2 falls below the on-site energy difference $\sim\Delta$. On the other hand, in DSC regimes of the present light-matter model, the effective coupling ξ (mass m_{eff}) decreases (increases) as the coupling g is increased, resulting in the suppression of the imaginary part of t_2. Since the on-site energy difference always remains to be $\sim\Delta$, the reentrant transition is expected to occur in DSC regimes as found in Fig. 1.

We expect that our analyses should be of relevance to recent experiments realizing strong light-matter interactions between low-dimensional materials and cavity photons [42,43,73,87–90,92]. In addition to condensed-matter systems, our consideration is also relevant to circuit QED ar-

chitectures, which can simulate single-electron Hamiltonians with periodic potentials [135,136]. We expect that geometrical and topological phenomena revealed by the present analyses can be explored by coupling these experimental systems to a chiral cavity/resonator or waveguide [54,55].

In summary, we developed a faithful and efficient theoretical framework to analyze geometry and topology in ultrastrongly coupled quantum light-matter systems. We applied our general approach to the concrete model of massive Dirac fermions on honeycomb lattice potential and revealed its complete phase diagram (Fig. 1), featuring the cavity-induced topological phase transition and its reentrant behavior in genuinely nonperturbative regimes. The suppression of the topological phase in deep strong-coupling regimes originates from intrinsic renormalizations of the electron mass and the effective coupling strength, and it should be a general feature of cavity QED materials. We expect that our results are of relevance to a wide range of systems not only in cavity QED materials, but also in circuit QED [137,138] and waveguide QED [139].

APPENDIX A: DERIVATION OF THE TRANSFORMED HAMILTONIAN FOR A SINGLE CAVITY MODE WITH ARBITRARY POLARIZATION

We provide here the derivation of the Hamiltonian (8) obtained after the asymptotically decoupling (AD) unitary transformation in the case of a single cavity mode with arbitrary polarization. Specifically, we start from the general two-dimensional cavity QED Hamiltonian in the Coulomb gauge (1):

$$\hat{H}_C = \frac{(\hat{\boldsymbol{p}} - q\hat{\boldsymbol{A}})^2}{2m} + V(\boldsymbol{r}) + \hbar\omega_c\left(\hat{a}^\dagger \hat{a} + \frac{1}{2}\right), \quad \text{(A1)}$$

$$\hat{\boldsymbol{A}} = A_0[(u\boldsymbol{e} + v\boldsymbol{e}^*)\hat{a} + (u^*\boldsymbol{e}^* + v^*\boldsymbol{e})\hat{a}^\dagger], \quad \text{(A2)}$$

where we expand the polarization vector $\boldsymbol{f}$ in Eq. (1) by the circular polarization vectors $\boldsymbol{e} = (1, -i)^{\mathrm{T}}/\sqrt{2}$ and $\boldsymbol{e}^* = (1, i)^{\mathrm{T}}/\sqrt{2}$. Here, u and v are arbitrary complex numbers that satisfy $|u|^2 + |v|^2 = 1$. We can take u and v to be real numbers without loss of generality; this is always possible by using a certain spatial rotation, $p_{x(y)} \mapsto p_{x(y)} \cos\theta + (-)p_{y(x)} \sin\theta$, and a $U(1)$ gauge transformation, $\hat{a} \mapsto e^{i\alpha}\hat{a}$. We note that the case of the circular polarization discussed in the main text corresponds to the choice of $u = 1$, $v = 0$.

To derive the expression of the transformed Hamiltonian, we first diagonalize the quadratic part, $q^2\hat{\boldsymbol{A}}^2/2m + \hbar\omega_c(\hat{a}^\dagger\hat{a} + 1/2)$, via the Bogoliubov transformation and rewrite the Hamiltonian (A1) as

$$\hat{H}_C = \frac{\hat{\boldsymbol{p}}^2}{2m} + V(\boldsymbol{r}) + \hbar\Omega\left(\hat{b}^\dagger\hat{b} + \frac{1}{2}\right)$$
$$- \frac{qA_0}{m}\hat{\boldsymbol{p}} \cdot \begin{pmatrix} \frac{u+v}{\sqrt{2}}\sqrt{\frac{\omega_{Ac}}{\Omega}}(\hat{b}^\dagger + \hat{b}) \\ i\frac{u-v}{\sqrt{2}}\sqrt{\frac{\Omega}{\omega_{Ac}}}(\hat{b}^\dagger - \hat{b}) \end{pmatrix}, \quad \text{(A3)}$$

$$\omega_{Ac} = (1 - 2uv)\omega_A + \omega_c, \quad \text{(A4)}$$

$$\Omega = \sqrt{(\omega_A + \omega_c)^2 - (2uv\omega_A)^2}, \quad \text{(A5)}$$

$$\omega_A = \frac{q^2 A_0^2}{m\hbar}, \quad \text{(A6)}$$

where $b^{(\dagger)}$ is a squeezed annihilation (creation) operator defined by

$$\hat{b}^\dagger + \hat{b} = \sqrt{\frac{\Omega}{\omega_{Ac}}}(\hat{a}^\dagger + \hat{a}), \quad \text{(A7)}$$

$$\hat{b}^\dagger - \hat{b} = \sqrt{\frac{\omega_{Ac}}{\Omega}}(\hat{a}^\dagger - \hat{a}). \quad \text{(A8)}$$

We then use the unitary transformation $\hat{U}$ defined by

$$\hat{U} = \exp\left(-ix_\Omega\frac{\hat{\boldsymbol{p}}}{\hbar} \cdot \hat{\boldsymbol{\rho}}\right), \quad \text{(A9)}$$

$$x_\Omega = \sqrt{\frac{\hbar}{m\Omega}}, \quad \text{(A10)}$$

$$\hat{\boldsymbol{\rho}} = \begin{pmatrix} \hat{\rho}_x \\ \hat{\rho}_y \end{pmatrix} = \begin{pmatrix} \lambda_+ i\frac{\hat{b}^\dagger - \hat{b}}{\sqrt{2}} \\ -\lambda_- \frac{\hat{b}^\dagger + \hat{b}}{\sqrt{2}} \end{pmatrix}, \quad \text{(A11)}$$

$$\lambda_\pm = \sqrt{\frac{\omega_A(1 \pm 2uv)}{\omega_A(1 \pm 2uv) + \omega_c}} \operatorname{sgn}(u \pm v). \quad \text{(A12)}$$

This unitary transformation $\hat{U}$ acts on the electron position operator $\boldsymbol{r}$ and the annihilation operator $\hat{b}$ via

$$\hat{U}^\dagger \boldsymbol{r}\hat{U} = \boldsymbol{r} + x_\Omega\hat{\boldsymbol{\rho}} + \frac{\hbar\omega_A}{m\Omega^2}(u^2 - v^2)\frac{\hat{\boldsymbol{p}} \times \boldsymbol{e}_z}{2\hbar}, \quad \text{(A13)}$$

$$\hat{U}^\dagger \hat{b}\hat{U} = \hat{b} + \frac{x_\Omega}{\sqrt{2}\hbar}(\lambda_+\hat{p}_x + i\lambda_-\hat{p}_y), \quad \text{(A14)}$$

where the last term on the RHS of Eq. (A13) originates from the noncommutativity between $\hat{\rho}_x$ and $\hat{\rho}_y$, i.e., $[\hat{\rho}_x, \hat{\rho}_y] = i(\omega_A/\Omega)(u^2 - v^2)$. Using these relations, we finally arrive at

the following transformed Hamiltonian $\hat{H}^U = \hat{U}^\dagger\hat{H}_C\hat{U}$:

$$\hat{H}^U = \frac{\hat{p}_x^2}{2m_{x,\text{eff}}} + \frac{\hat{p}_y^2}{2m_{y,\text{eff}}} + \hbar\Omega\left(\hat{b}^\dagger\hat{b} + \frac{1}{2}\right)$$
$$+ V\left(\boldsymbol{r} + x_\Omega\hat{\boldsymbol{\rho}} + \frac{\hbar\omega_A}{m\Omega^2}(u^2 - v^2)\frac{\hat{\boldsymbol{p}} \times \boldsymbol{e}_z}{2\hbar}\right), \quad \text{(A15)}$$

$$\frac{m_{x,\text{eff}}}{m} = \frac{\omega_A(1 + 2uv) + \omega_c}{\omega_c}, \quad \frac{m_{y,\text{eff}}}{m} = \frac{\omega_A(1 - 2uv) + \omega_c}{\omega_c}, \quad \text{(A16)}$$

which gives a generalization of Eq. (8) in the main text. We note that the Hamiltonian in the AD frame (A15) has a similar structure to Eq. (8). Thus, our formalism of evaluating physical observables and understanding of topological properties can also be applied to this case.

APPENDIX B: ASYMPTOTICALLY DECOUPLING UNITARY TRANSFORMATION FOR MULTIPLE CIRCULARLY POLARIZED CAVITY MODES

We extend here the AD unitary transformation in the main text to the system with multiple circularly polarized cavity modes, which is described by the following Coulomb-gauge Hamiltonian:

$$\hat{H}_C = \frac{(\hat{\boldsymbol{p}} - q\hat{\boldsymbol{A}})^2}{2m} + V(\boldsymbol{r}) + \sum_{i=1}^N \hbar\omega_i\hat{a}_i^\dagger\hat{a}_i + \sum_{j=1}^M \hbar v_j\hat{b}_j^\dagger\hat{b}_j, \quad \text{(B1)}$$

$$\hat{\boldsymbol{A}} = \sum_{i=1}^N f_i(\boldsymbol{e}\hat{a}_i + \boldsymbol{e}^*\hat{a}_i^\dagger) + \sum_{j=1}^M g_j(\boldsymbol{e}^*\hat{b}_j + \boldsymbol{e}\hat{b}_j^\dagger), \quad \text{(B2)}$$

where $\boldsymbol{e} = (1, -i)^{\mathrm{T}}/\sqrt{2}$, and $\hat{a}_i^{(\dagger)}$ and $\hat{b}_j^{(\dagger)}$ are the annihilation (creation) operators for the left and right circularly polarized modes with mode amplitudes $f_i, g_j \in \mathbb{R}$, respectively.

To diagonalize the quadratic part, $\hat{H}_{\text{quad}} = q^2\hat{\boldsymbol{A}}^2/2m + \sum_i \hbar\omega_i\hat{a}_i^\dagger\hat{a}_i + \sum_j \hbar v_j\hat{b}_j^\dagger\hat{b}_j$, we introduce the following conjugate pairs of variables:

$$\hat{r}_i = \begin{cases} \frac{\hat{a}_i^\dagger + \hat{a}_i}{\sqrt{2}} & (i = 1, \ldots, N), \\ \frac{\hat{b}_{i-N}^\dagger + \hat{b}_{i-N}}{\sqrt{2}} & (i = N+1, \ldots, N+M), \end{cases} \quad \text{(B3)}$$

$$\hat{q}_i = \begin{cases} i\frac{\hat{a}_i^\dagger - \hat{a}_i}{\sqrt{2}} & (i = 1, \ldots, N), \\ i\frac{\hat{b}_{i-N}^\dagger - \hat{b}_{i-N}}{\sqrt{2}} & (i = N+1, \ldots, N+M). \end{cases} \quad \text{(B4)}$$

In this representation, the quadratic part can be expressed as

$$\hat{H}_{\text{quad}} = \frac{\hbar}{2}\hat{\boldsymbol{r}}^T A\hat{\boldsymbol{r}} + \frac{\hbar}{2}\hat{\boldsymbol{q}}^T B\hat{\boldsymbol{q}}, \quad \text{(B5)}$$

$$A = \frac{q^2}{m\hbar}\boldsymbol{w}_1\boldsymbol{w}_1^T + \operatorname{diag}(\omega_1, \ldots, \omega_N, v_1, \ldots, v_M), \quad \text{(B6)}$$

$$B = \frac{q^2}{m\hbar}\boldsymbol{w}_2\boldsymbol{w}_2^T + \operatorname{diag}(\omega_1, \ldots, \omega_N, v_1, \ldots, v_M), \quad \text{(B7)}$$

where $\hat{\boldsymbol{r}}$ and $\hat{\boldsymbol{q}}$ denote $(\hat{r}_1, \ldots, \hat{r}_{N+M})^{\mathrm{T}}$ and $(\hat{q}_1, \ldots, \hat{q}_{N+M})^{\mathrm{T}}$, respectively. Here, we define the $(N + M)$-dimensional vectors $\boldsymbol{w}_1$ and $\boldsymbol{w}_2$ by $\boldsymbol{w}_1 = (f_1, \ldots, f_N, g_1 \ldots, g_M)$ and

$\boldsymbol{w}_2 = (f_1, \ldots, f_N, -g_1 \ldots, -g_M)$. Since A and B are both symmetric and positive-definite, there exists an $(N+M)$-dimensional real matrix P that satisfies $P^T A P = P^{-1} B P^{-T} =$ $\mathrm{diag}(\Omega_1, \ldots, \Omega_{N+M})$. One can confirm this by decomposing P into $P = B^{\frac{1}{2}} O D$, where O is an orthogonal matrix that diagonalizes $B^{\frac{1}{2}} A B^{\frac{1}{2}}$, and D is a diagonal matrix defined by $D = (O^T B^{\frac{1}{2}} A B^{\frac{1}{2}} O)^{-\frac{1}{4}}$. After replacing the conjugate pairs of variables via $\hat{\boldsymbol{r}} = P \hat{\boldsymbol{r}}'$ and $\hat{\boldsymbol{q}} = P^{-T} \hat{\boldsymbol{q}}'$, and introducing the corresponding annihilation (creation) operators $\hat{c}_i^{(\dagger)} = [\hat{r}_i' + (-)i\hat{q}_i']/\sqrt{2}$, we arrive at the following expression of the Coulomb gauge Hamiltonian (B1):

$$\hat{H}_C = \frac{\boldsymbol{p}^2}{2m} - \frac{q\hat{\boldsymbol{A}}}{m} \cdot \hat{\boldsymbol{p}} + V(\boldsymbol{r}) + \sum_{i=1}^{N+M} \hbar \Omega_i \hat{c}_i^\dagger \hat{c}_i, \quad \text{(B8)}$$

$$\hat{\boldsymbol{A}} = \sum_{i=1}^{N+M} [(u_i \boldsymbol{e} + v_i \boldsymbol{e}^*)\hat{c}_i + (u_i \boldsymbol{e}^* + v_i \boldsymbol{e})\hat{c}_i^\dagger], \quad \text{(B9)}$$

where u_i and v_i are defined by $(u_1, \ldots, u_{N+M})^T = \frac{1}{2}(P^T \boldsymbol{w}_1 + P^{-1} \boldsymbol{w}_2)$ and $(v_1, \ldots, v_{N+M})^T = \frac{1}{2}(P^T \boldsymbol{w}_1 - P^{-1} \boldsymbol{w}_2)$. We introduce the AD transformation $\hat{U}$ by

$$\hat{U} = \exp\left(-i\frac{\hat{\boldsymbol{p}}}{\hbar} \cdot \sum_{i=1}^{N+M} \hat{\boldsymbol{\rho}}_i\right), \quad \text{(B10)}$$

$$\hat{\boldsymbol{\rho}}_i = \frac{q}{m\Omega_i}(u_i \hat{\boldsymbol{\pi}}_i + v_i \hat{\boldsymbol{\pi}}_i'), \quad \text{(B11)}$$

where $\hat{\boldsymbol{\pi}}_i = -ie\hat{c}_i + ie^*\hat{c}_i^\dagger$ and $\hat{\boldsymbol{\pi}}_i' = -ie^*\hat{c}_i + ie\hat{c}_i^\dagger$. Using the above relations, we finally obtain the following transformed Hamiltonian $\hat{H}^U = \hat{U}^\dagger \hat{H}_C \hat{U}$:

$$\hat{H}^U = \frac{\boldsymbol{p}^2}{2m_{\mathrm{eff}}} + \sum_{i=1}^{N+M} \hbar \Omega_i \hat{c}_i^\dagger \hat{c}_i$$

$$+ V\left(\boldsymbol{r} + \sum_{i=1}^{N+M} \hat{\boldsymbol{\rho}}_i + \frac{\eta}{2\hbar} \boldsymbol{p} \times \boldsymbol{e}_z\right), \quad \text{(B12)}$$

$$m_{\mathrm{eff}} = m\left[1 + \frac{q^2}{m\hbar}\left(\sum_{i=1}^N \frac{f_i^2}{\omega_i} + \sum_{j=1}^M \frac{g_j^2}{v_j}\right)\right], \quad \text{(B13)}$$

$$\eta = \frac{q^2}{m^2} \frac{\sum_{i=1}^N \frac{f_i^2}{\omega_i^2} - \sum_{j=1}^M \frac{g_j^2}{v_j^2}}{\left[1 + \frac{q^2}{m\hbar}\left(\sum_{i=1}^N \frac{f_i^2}{\omega_i} + \sum_{j=1}^M \frac{g_j^2}{v_j}\right)\right]^2}. \quad \text{(B14)}$$

Again, the Hamiltonian in the AD frame (B12) has a similar structure as Eq. (8), and our formalism and understandings of topological properties can be similarly applied.

APPENDIX C: DERIVATION OF THE EXPRESSIONS FOR QUANTUM GEOMETRICAL QUANTITIES IN THE TRANSFORMED FRAME

We next derive the expressions of quantum geometrical quantities, including Berry curvature [see Eq. (12) in the main text], Berry connection, and quantum metric in the frame of reference after the AD unitary transformation. To this end, we first recall that the Bloch states in the Coulomb gauge can be related to the AD-frame counterparts by $|\psi_{n\boldsymbol{k}}^C\rangle = \hat{U}|\psi_{n\boldsymbol{k}}^U\rangle$ with $\hat{U} = \exp(-i\xi \frac{\boldsymbol{p}}{\hbar} \cdot \hat{\boldsymbol{\pi}})$. Thus, the periodic parts of these Bloch states, $|u_{n\boldsymbol{k}}^{C(U)}\rangle = e^{-i\boldsymbol{k}\boldsymbol{r}}|\psi_{n\boldsymbol{k}}^{C(U)}\rangle$, satisfy the following equality:

$$|u_{n\boldsymbol{k}}^C\rangle = e^{-i\boldsymbol{k}\boldsymbol{r}} \hat{U} e^{i\boldsymbol{k}\boldsymbol{r}} |u_{n\boldsymbol{k}}^U\rangle = \exp\left(-i\xi \frac{\boldsymbol{p} + \hbar \boldsymbol{k}}{\hbar} \cdot \hat{\boldsymbol{\pi}}\right) |u_{n\boldsymbol{k}}^U\rangle. \quad \text{(C1)}$$

To take the derivatives of Eq. (C1) with respect to k_x or k_y, we must pay attention to the fact that the operators $\hat{\pi}_x$ and $\hat{\pi}_y$ do not commute with each other, but satisfy $[\hat{\pi}_x, \hat{\pi}_y] = i$. It is thus useful to first employ the Baker-Campbell-Hausdorff formula and bring the term containing k_x (or k_y) to the right of Eq. (C1) as

$$|u_{n\boldsymbol{k}}^C\rangle = e^{-i\xi \frac{p_y + \hbar k_y}{\hbar} \hat{\pi}_y} e^{-i\xi \frac{p_x + \hbar k_x}{\hbar} \hat{\pi}_x} e^{-\frac{i\xi^2}{2\hbar^2}(p_x + \hbar k_x)(p_y + \hbar k_y)} |u_{n\boldsymbol{k}}^U\rangle \quad \text{(C2)}$$

$$= e^{-i\xi \frac{p_x + \hbar k_x}{\hbar} \hat{\pi}_x} e^{-i\xi \frac{p_y + \hbar k_y}{\hbar} \hat{\pi}_y} e^{\frac{i\xi^2}{2\hbar^2}(p_x + \hbar k_x)(p_y + \hbar k_y)} |u_{n\boldsymbol{k}}^U\rangle. \quad \text{(C3)}$$

We can now take the derivatives of Eq. (C1) with respect to k_x and k_y as follows:

$$\partial_{k_x}|u_{n\boldsymbol{k}}^C\rangle = \exp\left(-i\xi \frac{\boldsymbol{p} + \hbar \boldsymbol{k}}{\hbar} \cdot \hat{\boldsymbol{\pi}}\right)$$
$$\times \left[-i\xi \hat{\pi}_x - \frac{i\xi^2}{2\hbar}(p_y + \hbar k_y) + \partial_{k_x}\right]|u_{n\boldsymbol{k}}^U\rangle, \quad \text{(C4)}$$

$$\partial_{k_y}|u_{n\boldsymbol{k}}^C\rangle = \exp\left(-i\xi \frac{\boldsymbol{p} + \hbar \boldsymbol{k}}{\hbar} \cdot \hat{\boldsymbol{\pi}}\right)$$
$$\times \left[-i\xi \hat{\pi}_y + \frac{i\xi^2}{2\hbar}(p_x + \hbar k_x) + \partial_{k_y}\right]|u_{n\boldsymbol{k}}^U\rangle. \quad \text{(C5)}$$

The resulting expressions of Berry connection $\boldsymbol{A}_n^C(\boldsymbol{k}) = i\langle u_{n\boldsymbol{k}}^C|\nabla_{\boldsymbol{k}} u_{n\boldsymbol{k}}^C\rangle$ and Berry curvature are

$$\boldsymbol{A}_n^C(\boldsymbol{k}) = i\langle u_{n\boldsymbol{k}}^U|\nabla_{\boldsymbol{k}} u_{n\boldsymbol{k}}^U\rangle + \xi\langle \psi_{n\boldsymbol{k}}^U|\hat{\boldsymbol{\pi}}|\psi_{n\boldsymbol{k}}^U\rangle + \frac{\xi^2}{2\hbar}\langle \psi_{n\boldsymbol{k}}^U|\hat{\boldsymbol{p}} \times \boldsymbol{e}_z|\psi_{n\boldsymbol{k}}^U\rangle, \quad \text{(C6)}$$

$$B_n^C(\boldsymbol{k}) = i\left(\langle \partial_{k_x} u_{n\boldsymbol{k}}^U|\partial_{k_y} u_{n\boldsymbol{k}}^U\rangle - \langle \partial_{k_y} u_{n\boldsymbol{k}}^U|\partial_{k_x} u_{n\boldsymbol{k}}^U\rangle\right)$$
$$+ \xi\left[\nabla_{\boldsymbol{k}} \times \langle \psi_{n\boldsymbol{k}}^U|\hat{\boldsymbol{\pi}}|\psi_{n\boldsymbol{k}}^U\rangle\right]_{k_z} - \frac{\xi^2}{2\hbar}\nabla_{\boldsymbol{k}} \cdot \langle \psi_{n\boldsymbol{k}}^U|\hat{\boldsymbol{p}}|\psi_{n\boldsymbol{k}}^U\rangle. \quad \text{(C7)}$$

For the sake of completeness, we also provide the expression of the quantum geometric tensor $\mathfrak{G}^C(\boldsymbol{k})$ defined by

$$\mathfrak{G}_{n,ij}^C(\boldsymbol{k}) = \langle \partial_{k_i} u_{n\boldsymbol{k}}^C|\left[1 - |u_{n\boldsymbol{k}}^C\rangle\langle u_{n\boldsymbol{k}}^C|\right]|\partial_{k_j} u_{n\boldsymbol{k}}^C\rangle \quad (i, j = x, y). \quad \text{(C8)}$$

We note that the quantum metric $g_{n,ij}^C(\boldsymbol{k})$ is given by the real part of the quantum geometric tensor. Using Eqs. (C4) and (C5), we can rewrite the quantum geometric tensor (C8)
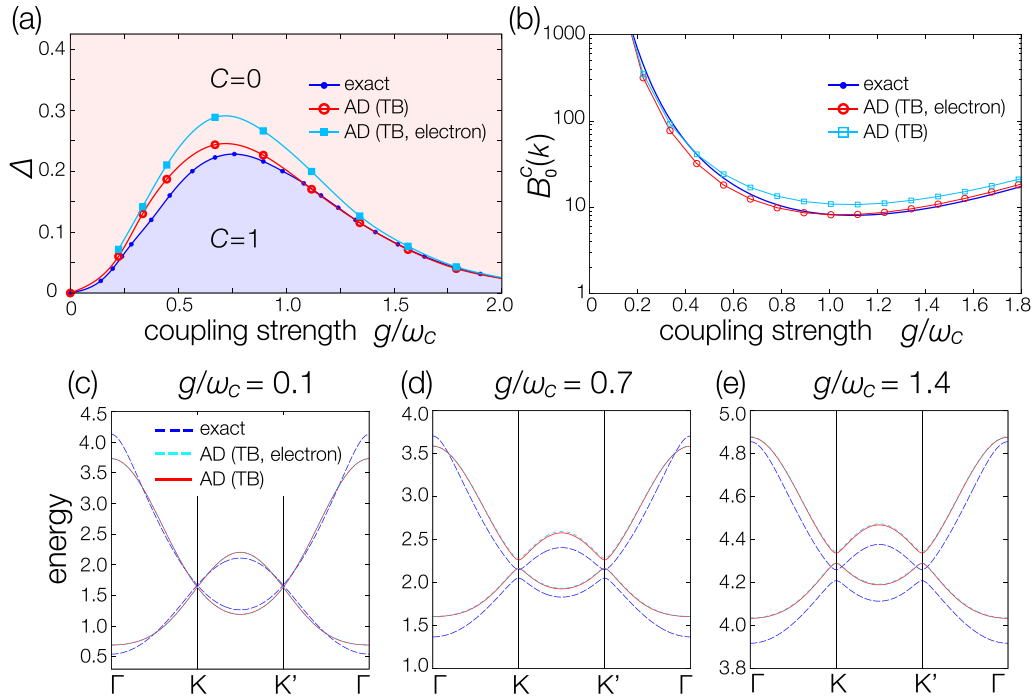
FIG. 5. (a)–(e) Comparisons of the results obtained from the electron-photon tight-binding model in the transformed frame [Eq. (11) in the main text] and its electron-part Hamiltonian (D1). Each panel corresponds to (a) the phase boundary, (b) Berry curvature, and (c)–(e) energy spectra of the honeycomb model considered in the main text. Parameters are the same as in Figs. 1, 3, and 4 in the main text.

in terms of the AD-frame Bloch states as

$$
\begin{aligned}
\mathfrak{G}_{n,ij}(\boldsymbol{k}) &= \langle \partial_{k_i} u^U_{n\boldsymbol{k}} | \big[1 - |u^U_{n\boldsymbol{k}}\rangle\langle u^U_{n\boldsymbol{k}}| \big] | \partial_{k_j} u^U_{n\boldsymbol{k}}\rangle + \langle u^U_{n\boldsymbol{k}} | \left(i\xi\hat{\pi}_i + \frac{i\xi^2}{2\hbar}[(\boldsymbol{p}+\hbar\boldsymbol{k})\times\boldsymbol{e}_z]_i \right) \big[1 - |u^U_{n\boldsymbol{k}}\rangle\langle u^U_{n\boldsymbol{k}}| \big] | \partial_{k_j} u^U_{n\boldsymbol{k}}\rangle \\
&\quad + \langle \partial_{k_i} u^U_{n\boldsymbol{k}} | \big[1 - |u^U_{n\boldsymbol{k}}\rangle\langle u^U_{n\boldsymbol{k}}| \big] \left(-i\xi\hat{\pi}_j - \frac{i\xi^2}{2\hbar}[(\boldsymbol{p}+\hbar\boldsymbol{k})\times\boldsymbol{e}_z]_j \right) | u^U_{n\boldsymbol{k}}\rangle \\
&\quad + \langle u^U_{n\boldsymbol{k}} | \left(i\xi\hat{\pi}_i + \frac{i\xi^2}{2\hbar}[(\boldsymbol{p}+\hbar\boldsymbol{k})\times\boldsymbol{e}_z]_i \right) \left(-i\xi\hat{\pi}_j - \frac{i\xi^2}{2\hbar}[(\boldsymbol{p}+\hbar\boldsymbol{k})\times\boldsymbol{e}_z]_j \right) | u^U_{n\boldsymbol{k}}\rangle \\
&\quad - \langle u^U_{n\boldsymbol{k}} | \left(i\xi\hat{\pi}_i + \frac{i\xi^2}{2\hbar}[(\boldsymbol{p}+\hbar\boldsymbol{k})\times\boldsymbol{e}_z]_i \right) | u^U_{n\boldsymbol{k}}\rangle\langle u^U_{n\boldsymbol{k}}| \left(-i\xi\hat{\pi}_j - \frac{i\xi^2}{2\hbar}[(\boldsymbol{p}+\hbar\boldsymbol{k})\times\boldsymbol{e}_z]_j \right) | u^U_{n\boldsymbol{k}}\rangle.
\end{aligned}
\tag{C9}
$$

In Eqs. (C6), (C7), and (C9), the first term in each equation gives the dominant contribution which can be efficiently evaluated by employing the electron-only tight-binding description (13). Nevertheless, we emphasize that it is also possible to include higher-order terms to systematically improve quantitative accuracy when necessary.

APPENDIX D: EFFECTS OF ELECTROMAGNETIC FLUCTUATIONS IN THE TIGHT-BINDING MODEL

We examine here the effects of electromagnetic fluctuations $\hat{\mu}_{ij}$ in the transformed frame by comparing the results of the electron-photon tight-binding Hamiltonian [Eq. (11) in the main text] and its electron-only part,

$$
\hat{H}^U_{\text{TB,mat}} = \sum_{\langle ij\rangle} t_{ij}|w_i\rangle\langle w_j|.
\tag{D1}
$$

Figure 5 compares the results obtained from these two tight-binding Hamiltonians. Each panel corresponds to (a) the phase boundary, (b) Berry curvature, and (c)–(e) energy spectra of the honeycomb model, respectively. The parameters are chosen in the same manner as in Figs. 1, 3, and 4 in the main text. These comparisons demonstrate that the electromagnetic fluctuations in the transformed frame only lead to minor modifications, and qualitative features in the low-energy physics can be well captured simply by its electron-part Hamiltonian (D1), where the photon degrees of freedom are completely eliminated.

APPENDIX E: DETAILS OF THE CONVENTIONAL ANALYSIS USING THE MINIMALLY COUPLED DIRAC HAMILTONIAN

We provide the technical details about the conventional analysis using the minimally coupled Dirac Hamiltonian
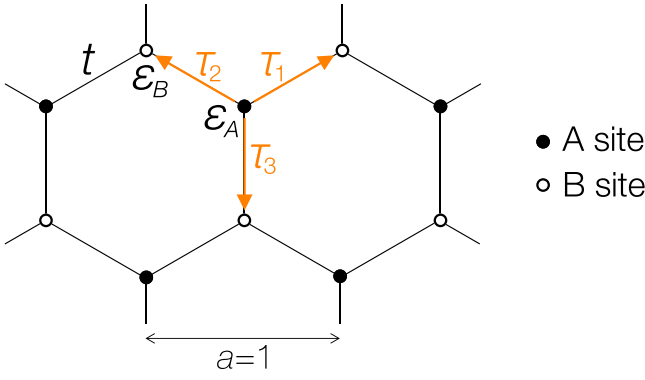
FIG. 6. Honeycomb tight-binding model in Eq. (E1). Solid and open points represent A- and B-sublattice sites, respectively. Here, $\varepsilon_{A(B)}$ is the on-site energy of each sublattice A (B), and t is the hopping amplitude to the nearest neighbors.

considered in the main text. To derive the Dirac Hamiltonian, we start from the following honeycomb tight-binding model constructed from $\hat{H} = p^2/2m + V(\boldsymbol{r})$ with the potential (14) in the main text:

$$\hat{H} = \sum_i \left(\varepsilon_A |w_{i,A}^0\rangle\langle w_{i,A}^0| + \varepsilon_B |w_{i,B}^0\rangle\langle w_{i,B}^0| \right)$$
$$+ \sum_{\text{1st nearest neighbors}} t \left(|w_{i,A}^0\rangle\langle w_{j,B}^0| + |w_{j,B}^0\rangle\langle w_{i,A}^0| \right), \quad \text{(E1)}$$

where $|w_{i,A(B)}^0\rangle$ denotes the Wannier orbital localized at the sublattice A (B) in the ith unit cell. Here, $\varepsilon_{A(B)}$ is the on-site energy of the sublattice A (B), and t is the hopping amplitude to the first nearest neighbors (see also Fig. 6 below). In the basis of two-component spinors $(|\psi_{\boldsymbol{k},A}\rangle, |\psi_{\boldsymbol{k},B}\rangle)$ corresponding to the Bloch states on the two sublattices, this tight-binding Hamiltonian becomes

$$\hat{H}(\boldsymbol{k}) = \frac{\varepsilon_A + \varepsilon_B}{2}\hat{I}_2 + \frac{\varepsilon_A - \varepsilon_B}{2}\hat{\sigma}_z$$
$$+ \sum_{i=1,2,3} [\cos(\boldsymbol{k} \cdot \boldsymbol{\tau}_i)\hat{\sigma}_x - \sin(\boldsymbol{k} \cdot \boldsymbol{\tau}_i)\hat{\sigma}_y], \quad \text{(E2)}$$

where $\hat{\sigma}_i$ ($i = x, y, z$) are the Pauli matrices and $\boldsymbol{\tau}_i$ ($i = 1, 2, 3$) are the three displacement vectors from an A site to its three nearest-neighbor B sites. By expanding Eq. (E2) around the two Dirac points $[\boldsymbol{K} = \pm(\boldsymbol{b}_1/3 + \boldsymbol{b}_2/3)]$, we obtain the following massive Dirac Hamiltonians:

$$\hat{H}_{\text{Dirac}}(\boldsymbol{k}) = \frac{\varepsilon_A + \varepsilon_B}{2}\hat{I}_2 + \frac{\varepsilon_A - \varepsilon_B}{2}\hat{\sigma}_z$$
$$+ \frac{\sqrt{3}t}{2}(k_x\hat{\sigma}_x \pm k_y\hat{\sigma}_y). \quad \text{(E3)}$$

The minimally coupled Dirac Hamiltonian $\hat{H}_{\text{Dirac}}^A(\boldsymbol{k})$ can then be obtained after replacing the wave vector $\boldsymbol{k}$ in Eq. (E3) by $\boldsymbol{k} - (q/\hbar)\hat{\boldsymbol{A}}$:

$$\hat{H}_{\text{Dirac}}^A(\boldsymbol{k}) = \frac{\varepsilon_A + \varepsilon_B}{2}\hat{I}_2 + \frac{\varepsilon_A - \varepsilon_B}{2}\hat{\sigma}_z + \hbar\omega_c\hat{a}^\dagger\hat{a}$$
$$+ \frac{\sqrt{3}t}{2}\left[\left(k_x - \frac{q\hat{A}_x}{\hbar}\right)\hat{\sigma}_x \pm \left(k_y - \frac{q\hat{A}_y}{\hbar}\right)\hat{\sigma}_y \right], \quad \text{(E4)}$$

where $\hat{\boldsymbol{A}}$ is the vector potential operator defined by Eq. (2) in the main text. In the phase diagram of the honeycomb model (Fig. 1 in the main text), we determine the phase boundary of the minimally coupled Dirac Hamiltonian (E4) by locating the coupling g at which the energy gap above the lowest electron-polariton band closes. We also evaluate the Chern number (inset of Fig. 1 in the main text) by integrating Berry curvature of the lowest electron-polariton band over a sufficiently large area and summing up the contributions from the two Dirac points.

APPENDIX F: DETAILS OF THE EXACT ANALYSIS

We provide here the technical details about the exact analysis performed in the main text. To obtain exact results at ultrastrong coupling strengths, we use the continuum Hamiltonian in the AD frame (8) as

$$\hat{H}^U = \frac{\hat{\boldsymbol{p}}^2}{2m_{\text{eff}}} + \hbar\Omega\left(\hat{a}^\dagger\hat{a} + \frac{1}{2}\right)$$
$$+ \sum_{\boldsymbol{G}} V_{\boldsymbol{G}} e^{i\boldsymbol{G}\boldsymbol{r}} e^{\frac{i\xi^2}{2\hbar}\boldsymbol{G}\cdot\hat{\boldsymbol{p}}\times\boldsymbol{e}_z} e^{i\xi\boldsymbol{G}\cdot\hat{\boldsymbol{\pi}}}. \quad \text{(F1)}$$

The matrix elements of $\hat{H}_{\boldsymbol{k}}^U \equiv e^{-i\boldsymbol{k}\boldsymbol{r}}\hat{H}^U e^{i\boldsymbol{k}\boldsymbol{r}}$ with respect to $|\boldsymbol{K}\otimes n\rangle$, which is the tensor product of the plane wave with wave vector $\boldsymbol{K} \in \mathbb{Z}\boldsymbol{b}_1 + \mathbb{Z}\boldsymbol{b}_2$ and photon number eigenstate $|n\rangle$, are given by

$$\langle \boldsymbol{K}\otimes n|\hat{H}_{\boldsymbol{k}}^U|\boldsymbol{K}'\otimes n'\rangle$$
$$= \frac{\hbar^2(\boldsymbol{K}+\boldsymbol{k})^2}{2m_{\text{eff}}}\delta_{\boldsymbol{K},\boldsymbol{K}'} + \hbar\Omega\left(n + \frac{1}{2}\right)\delta_{nn'}$$
$$+ \sum_{\boldsymbol{G}} V_{\boldsymbol{G}} e^{\frac{i\xi^2}{2}[\boldsymbol{G}\times(\boldsymbol{K}+\boldsymbol{k})]_z}\delta_{\boldsymbol{K},\boldsymbol{K}'+\boldsymbol{G}} \times \langle n|e^{i\xi\boldsymbol{G}\cdot\hat{\boldsymbol{\pi}}}|n'\rangle. \quad \text{(F2)}$$

We can perform the exact diagonalization of $\hat{H}_{\boldsymbol{k}}^U$ to obtain its spectrum and eigenstate $|u_{n\boldsymbol{k}}^U\rangle$ at the expense of high computational costs.

To evaluate the Berry curvature (12), we start with the equivalent expression (4) in the Coulomb gauge. We first rewrite it as

$$B_n^C(\boldsymbol{k}) = -2\,\text{Im}\sum_{m\neq n}\frac{\langle u_{n\boldsymbol{k}}^C|\partial_{k_x}\hat{H}_{\boldsymbol{k}}^C|u_{m\boldsymbol{k}}^C\rangle\langle u_{m\boldsymbol{k}}^C|\partial_{k_y}\hat{H}_{\boldsymbol{k}}^C|u_{n\boldsymbol{k}}^C\rangle}{(\varepsilon_{n\boldsymbol{k}} - \varepsilon_{m\boldsymbol{k}})^2}, \quad \text{(F3)}$$

where $\varepsilon_{n\boldsymbol{k}}$ is the nth eigenvalue of $\hat{H}_{\boldsymbol{k}}^C \equiv e^{-i\boldsymbol{k}\boldsymbol{r}}\hat{H}_C e^{i\boldsymbol{k}\boldsymbol{r}}$. Since $|u_{n\boldsymbol{k}}^C\rangle$ and $|u_{n\boldsymbol{k}}^U\rangle$ are related via Eq. (C1), we can rewrite $\langle u_{n\boldsymbol{k}}^C|\nabla\hat{H}_{\boldsymbol{k}}^C|u_{m\boldsymbol{k}}^C\rangle$ in Eq. (F3) in terms of Bloch states in the AD frame as

$$\langle u_{n\boldsymbol{k}}^C|\nabla\hat{H}_{\boldsymbol{k}}^C|u_{m\boldsymbol{k}}^C\rangle = \hbar\langle u_{n\boldsymbol{k}}^C|\left(\frac{\hat{\boldsymbol{p}} + \hbar\boldsymbol{k} - q\hat{\boldsymbol{A}}}{m}\right)|u_{m\boldsymbol{k}}^C\rangle \quad \text{(F4)}$$

$$= \hbar\langle u_{n\boldsymbol{k}}^U|\left(\frac{\hat{\boldsymbol{p}} + \hbar\boldsymbol{k}}{m_{\text{eff}}} - \frac{q\hat{\boldsymbol{A}}}{m}\right)|u_{m\boldsymbol{k}}^U\rangle. \quad \text{(F5)}$$

With Eqs. (F3) and (F5), we obtain the following expression of Berry curvature $B_n^C(\boldsymbol{k})$, which is used in evaluating the exact

Berry curvature in Fig. 3:

$$B_n^C(\boldsymbol{k}) = -2\hbar^2 \text{Im} \sum_{m \neq n} \frac{\langle u_{n\boldsymbol{k}}^U | \left(\frac{\hat{p}_x + \hbar k_x}{m_{\text{eff}}} - \frac{q\hat{A}_x}{m} \right) | u_{m\boldsymbol{k}}^U \rangle \langle u_{m\boldsymbol{k}}^U | \left(\frac{\hat{p}_y + \hbar k_y}{m_{\text{eff}}} - \frac{q\hat{A}_y}{m} \right) | u_{n\boldsymbol{k}}^U \rangle}{(\varepsilon_{n\boldsymbol{k}} - \varepsilon_{m\boldsymbol{k}})^2}. \tag{F6}$$

Finally, we compare the computational cost of the exact diagonalization (ED) method with our effective description based on the tight-binding model. In practice, to implement the numerical ED with the matrix elements (F2), we have to introduce a cutoff $N_c^{e(p)} \in \mathbb{Z}_{>0}$ for the electron (photon) states and consider the Hilbert space spanned by $|\boldsymbol{K} \otimes n\rangle = |m_1\boldsymbol{b}_1 + m_2\boldsymbol{b}_2 \otimes n'\rangle$ with $-N_c^e \leqslant m_i \leqslant N_c^e$ and $0 \leqslant n < N_c^p$. The dimension of the Hilbert space in the ED is then given by $D = (2N_c^e + 1)^2 \times N_c^p$, and the computational cost of each ED scales as $O(D^3)$. Meanwhile, the dimension of the Hilbert

space D' in our effective model (11) is $d_{\text{orb}} \times N_c^p$, where d_{orb} is the number of tight-binding orbitals in the unit cell. Since D' is much smaller than D, our framework allows one to significantly compress the relevant Hilbert space and to numerically evaluate physical quantities in a much more efficient way than the ED. For instance, in the massive honeycomb model explained in the main text, we can confirm the convergence of the energy spectra in the ED by choosing $N_c^e = 7, N_c^p = 4$ corresponding to $D = 900$, while in our effective model, it suffices to choose $d_{\text{orb}} = 2, N_c^p = 4$ corresponding to $D' = 8$.

[1] M. V. Berry, Proc. R. Soc. London **392**, 45 (1984).

[2] J. P. Provost and G. Vallee, Commun. Math. Phys. **76**, 289 (1980).

[3] D. Vanderbilt, *Berry Phases in Electronic Structure Theory* (Cambridge University Press, Cambridge, 2018).

[4] R. Resta, Ferroelectrics **136**, 51 (1992); Rev. Mod. Phys. **66**, 899 (1994).

[5] K. v. Klitzing, G. Dorda, and M. Pepper, Phys. Rev. Lett. **45**, 494 (1980).

[6] D. J. Thouless, M. Kohmoto, M. P. Nightingale, and M. den Nijs, Phys. Rev. Lett. **49**, 405 (1982).

[7] C. L. Kane and E. J. Mele, Phys. Rev. Lett. **95**, 226801 (2005).

[8] D. N. Sheng, Z. Y. Weng, L. Sheng, and F. D. M. Haldane, Phys. Rev. Lett. **97**, 036808 (2006).

[9] N. Nagaosa, J. Sinova, S. Onoda, A. H. MacDonald, and N. P. Ong, Rev. Mod. Phys. **82**, 1539 (2010).

[10] L. Tarruell, D. Greif, T. Uehlinger, G. Jotzu, and T. Esslinger, Nature (London) **483**, 302 (2012).

[11] J.-W. Rhim, K. Kim, and B.-J. Yang, Nature (London) **584**, 59 (2020).

[12] Y. Hwang, J.-W. Rhim, and B.-J. Yang, Nat. Commun. **12**, 6433 (2021).

[13] G. E. Topp, C. J. Eckhardt, D. M. Kennes, M. A. Sentef, and P. Törmä, Phys. Rev. B **104**, 064306 (2021).

[14] J. Ahn, G.-Y. Guo, N. Nagaosa, and A. Vishwanath, Nat. Phys. **18**, 290 (2022).

[15] M. Z. Hasan and C. L. Kane, Rev. Mod. Phys. **82**, 3045 (2010).

[16] X.-L. Qi and S.-C. Zhang, Rev. Mod. Phys. **83**, 1057 (2011).

[17] D. J. Thouless, Phys. Rev. B **27**, 6083 (1983).

[18] F. D. M. Haldane, Phys. Rev. Lett. **61**, 2015 (1988).

[19] L. Fu and C. L. Kane, Phys. Rev. B **74**, 195312 (2006).

[20] J. E. Moore and L. Balents, Phys. Rev. B **75**, 121306(R) (2007).

[21] A. P. Schnyder, S. Ryu, A. Furusaki, and A. W. W. Ludwig, Phys. Rev. B **78**, 195125 (2008).

[22] A. Kitaev, V. Lebedev, and M. Feigel'man, *Advances in Theoretical Physics: Landau Memorial Conference*, AIP Conf. Proc. 1134 (AIP, New York, 2009), pp. 22–30.

[23] J. C. Y. Teo and C. L. Kane, Phys. Rev. B **82**, 115120 (2010).

[24] F. Schäfer, T. Fukuhara, S. Sugawa, Y. Takasu, and Y. Takahashi, Nat. Rev. Phys. **2**, 411 (2020).

[25] M. Lohse, C. Schweizer, O. Zilberberg, M. Aidelsburger, and I. Bloch, Nat. Phys **12**, 350 (2016).

[26] N. Goldman, J. C. Budich, and P. Zoller, Nat. Phys **12**, 639 (2016).

[27] M. Aidelsburger, M. Atala, S. Nascimbène, S. Trotzky, Y.-A. Chen, and I. Bloch, Phys. Rev. Lett. **107**, 255301 (2011).

[28] G. Jotzu, M. Messer, R. Desbuquois, M. Lebrat, T. Uehlinger, D. Greif, and T. Esslinger, Nature (London) **515**, 237 (2014).

[29] A. M. Dudarev, R. B. Diener, I. Carusotto, and Q. Niu, Phys. Rev. Lett. **92**, 153005 (2004).

[30] A. Celi, P. Massignan, J. Ruseckas, N. Goldman, I. B. Spielman, G. Juzeliūnas, and M. Lewenstein, Phys. Rev. Lett. **112**, 043001 (2014).

[31] B. Song, L. Zhang, C. He, T. F. J. Poon, E. Hajiyev, S. Zhang, X.-J. Liu, and G.-B. Jo, Sci. Adv. **4**, eaao4748 (2018).

[32] L. Asteria, D. T. Tran, T. Ozawa, M. Tarnowski, B. S. Rem, N. Fläschner, K. Sengstock, N. Goldman, and C. Weitenberg, Nat. Phys. **15**, 449 (2019).

[33] M. Hafezi, E. A. Demler, M. D. Lukin, and J. M. Taylor, Nat. Phys. **7**, 907 (2011).

[34] T. Kitagawa, M. A. Broome, A. Fedrizzi, M. S. Rudner, E. Berg, I. Kassal, A. Aspuru-Guzik, E. Demler, and A. G. White, Nat. Commun. **3**, 882 (2012).

[35] L. Lu, J. D. Joannopoulos, and M. Soljačić, Nat. Photon **8**, 821 (2014).

[36] L.-H. Wu and X. Hu, Phys. Rev. Lett. **114**, 223901 (2015).

[37] L. J. Maczewsky, J. M. Zeuner, S. Nolte, and A. Szameit, Nat. Commun. **8**, 13756 (2017).

[38] S. Mukherjee, A. Spracklen, M. Valiente, E. Andersson, P. Öhberg, N. Goldman, and R. R. Thomson, Nat. Commun. **8**, 13918 (2017).

[39] T. Ozawa, H. M. Price, A. Amo, N. Goldman, M. Hafezi, L. Lu, M. C. Rechtsman, D. Schuster, J. Simon, O. Zilberberg, and I. Carusotto, Rev. Mod. Phys. **91**, 015006 (2019).

[40] A. Gianfrate, O. Bleu, L. Dominici, V. Ardizzone, M. De Giorgi, D. Ballarini, G. Lerario, K. W. West, L. N. Pfeiffer,

D. D. Solnyshkov, D. Sanvitto, and G. Malpuech, Nature (London) **578**, 381 (2020).

[41] A. A. Anappara, S. De Liberato, A. Tredicucci, C. Ciuti, G. Biasiol, L. Sorba, and F. Beltram, Phys. Rev. B **79**, 201303(R) (2009).

[42] G. Scalari, C. Maissen, D. Turčinková, D. Hagenmüller, S. De Liberato, C. Ciuti, C. Reichl, D. Schuh, W. Wegscheider, M. Beck, and J. Faist, Science **335**, 1323 (2012).

[43] C. Maissen, G. Scalari, F. Valmorra, M. Beck, J. Faist, S. Cibella, R. Leoni, C. Reichl, C. Charpentier, and W. Wegscheider, Phys. Rev. B **90**, 205309 (2014).

[44] S. Gambino, M. Mazzeo, A. Genco, O. Di Stefano, S. Savasta, S. Patanè, D. Ballarini, F. Mangione, G. Lerario, D. Sanvitto, and G. Gigli, ACS Photon. **1**, 1042 (2014).

[45] R. Chikkaraddy, B. de Nijs, F. Benz, S. J. Barrow, O. A. Scherman, E. Rosta, A. Demetriadou, P. Fox, O. Hess, and J. J. Baumberg, Nature (London) **535**, 127 (2016).

[46] A. Bayer, M. Pozimski, S. Schambeck, D. Schuh, R. Huber, D. Bougeard, and C. Lange, Nano Lett. **17**, 6340 (2017).

[47] M. Halbhuber, J. Mornhinweg, V. Zeller, C. Ciuti, D. Bougeard, R. Huber, and C. Lange, Nat. Photon. **14**, 675 (2020).

[48] A. Genco, A. Ridolfo, S. Savasta, S. Patanè, G. Gigli, and M. Mazzeo, Adv. Opt. Mater. **6**, 1800364 (2018).

[49] F. Yoshihara, T. Fuse, S. Ashhab, K. Kakuyanagi, S. Saito, and K. Semba, Nat. Phys. **13**, 44 (2017).

[50] J. Flick, M. Ruggenthaler, H. Appel, and A. Rubio, Proc. Natl. Acad. Sci. USA **114**, 3026 (2017).

[51] P. Forn-Díaz, L. Lamata, E. Rico, J. Kono, and E. Solano, Rev. Mod. Phys. **91**, 025005 (2019).

[52] A. Frisk Kockum, A. Miranowicz, S. De Liberato, S. Savasta, and F. Nori, Nat. Rev. Phys. **1**, 19 (2019).

[53] F. J. Garcia-Vidal, C. Ciuti, and T. W. Ebbesen, Science **373**, eabd0336 (2021).

[54] H. Hübener, U. De Giovannini, C. Schäfer, J. Andberger, M. Ruggenthaler, J. Faist, and A. Rubio, Nat. Mater. **20**, 438 (2021).

[55] J. C. Owens, M. G. Panetta, B. Saxberg, G. Roberts, S. Chakram, R. Ma, A. Vrajitoarea, J. Simon, and D. I. Schuster, Nat. Phys. **18**, 1048 (2022).

[56] F. Schlawin, D. M. Kennes, and M. A. Sentef, Appl. Phys. Rev. **9**, 011312 (2022).

[57] J. Bloch, A. Cavalleri, V. Galitski, M. Hafezi, and A. Rubio, Nature (London) **606**, 41 (2022).

[58] M. Ruggenthaler, N. Tancogne-Dejean, J. Flick, H. Appel, and A. Rubio, Nat. Rev. Chem. **2**, 0118 (2018).

[59] R. F. Ribeiro, L. A. Martínez-Martínez, M. Du, J. Campos-Gonzalez-Angulo, and J. Yuen-Zhou, Chem. Sci. **9**, 6325 (2018).

[60] J. Flick, N. Rivera, and P. Narang, Nanophotonics **7**, 1479 (2018).

[61] J. Flick, D. M. Welakuh, M. Ruggenthaler, H. Appel, and A. Rubio, ACS Photon. **6**, 2757 (2019).

[62] J. Galego, F. J. Garcia-Vidal, and J. Feist, Phys. Rev. X **5**, 041022 (2015).

[63] F. Herrera and F. C. Spano, Phys. Rev. Lett. **116**, 238301 (2016).

[64] T. Chervy, J. Xu, Y. Duan, C. Wang, L. Mager, M. Frerejean, J. A. W. Münninghoff, P. Tinnemans, J. A. Hutchison, C. Genet, A. E. Rowan, T. Rasing, and T. W. Ebbesen, Nano Lett. **16**, 7352 (2016).

[65] T. W. Ebbesen, Acc. Chem. Res. **49**, 2403 (2016).

[66] J. Feist, J. Galego, and F. J. Garcia-Vidal, ACS Photon. **5**, 205 (2018).

[67] A. Thomas, J. George, A. Shalabney, M. Dryzhakov, S. J. Varma, J. Moran, T. Chervy, X. Zhong, E. Devaux, C. Genet, J. A. Hutchison, and T. W. Ebbesen, Angew. Chem. Int. Ed. **55**, 11462 (2016).

[68] K. Stranius, M. Hertzog, and K. Börjesson, Nat. Commun. **9**, 2273 (2018).

[69] L. A. Martínez-Martínez, M. Du, R. F. Ribeiro, S. Kéna-Cohen, and J. Yuen-Zhou, J. Phys. Chem. Lett. **9**, 1951 (2018).

[70] L. A. Martínez-Martínez, E. Eizner, S. Kéna-Cohen, and J. Yuen-Zhou, J. Chem. Phys. **151**, 054106 (2019).

[71] D. Polak, R. Jayaprakash, T. P. Lyons, L. Á. Martínez-Martínez, A. Leventis, K. J. Fallon, H. Coulthard, D. G. Bossanyi, K. Georgiou, I. I. Anthony J. Petty, J. Anthony, H. Bronstein, J. Yuen-Zhou, A. I. Tartakovskii, J. Clark, and A. J. Musser, Chem. Sci. **11**, 343 (2020).

[72] B. Xiang, R. F. Ribeiro, M. Du, L. Chen, Z. Yang, J. Wang, J. Yuen-Zhou, and W. Xiong, Science **368**, 665 (2020).

[73] G. Scalari, C. Maissen, S. Cibella, R. Leoni, P. Carelli, F. Valmorra, M. Beck, and J. Faist, New J. Phys. **16**, 033005 (2014).

[74] F. Schlawin, A. Cavalleri, and D. Jaksch, Phys. Rev. Lett. **122**, 133602 (2019).

[75] J. B. Curtis, Z. M. Raines, A. A. Allocca, M. Hafezi, and V. M. Galitski, Phys. Rev. Lett. **122**, 167002 (2019).

[76] J. B. Curtis, A. Grankin, N. R. Poniatowski, V. M. Galitski, P. Narang, and E. Demler, Phys. Rev. Res. **4**, 013101 (2022).

[77] H. Gao, F. Schlawin, and D. Jaksch, Phys. Rev. B **104**, L140503 (2021).

[78] M. A. Sentef, M. Ruggenthaler, and A. Rubio, Sci. Adv. **4**, eaau6969 (2018).

[79] Y. Ashida, A. İmamoğlu, J. Faist, D. Jaksch, A. Cavalleri, and E. Demler, Phys. Rev. X **10**, 041027 (2020).

[80] P. Pilar, D. De Bernardis, and P. Rabl, Quantum **4**, 335 (2020).

[81] S. Latini, D. Shin, S. A. Sato, C. Schäfer, U. De Giovannini, H. Hübener, and A. Rubio, Proc. Natl. Acad. Sci. USA **118**, e2105618118 (2021).

[82] K. Lenk, J. Li, P. Werner, and M. Eckstein, arXiv:2205.05559.

[83] S. Smolka, W. Wuester, F. Haupt, S. Faelt, W. Wegscheider, and A. Imamoglu, Science **346**, 332 (2014).

[84] C. Ciuti, Phys. Rev. B **104**, 155307 (2021).

[85] V. Rokaj, M. Penz, M. A. Sentef, M. Ruggenthaler, and A. Rubio, Phys. Rev. Lett. **123**, 047202 (2019).

[86] V. Rokaj, M. Penz, M. A. Sentef, M. Ruggenthaler, and A. Rubio, Phys. Rev. B **105**, 205424 (2022).

[87] F. Appugliese, J. Enkner, G. L. Paravicini-Bagliani, M. Beck, C. Reichl, W. Wegscheider, G. Scalari, C. Ciuti, and J. Faist, Science **375**, 1030 (2022).

[88] Q. Zhang, M. Lou, X. Li, J. L. Reno, W. Pan, J. D. Watson, M. J. Manfra, and J. Kono, Nat. Phys. **12**, 1005 (2016).

[89] G. L. Paravicini-Bagliani, F. Appugliese, E. Richter, F. Valmorra, J. Keller, M. Beck, N. Bartolo, C. Rössler, T. Ihn, K. Ensslin, C. Ciuti, G. Scalari, and J. Faist, Nat. Phys. **15**, 186 (2019).

[90] J. Keller, G. Scalari, F. Appugliese, S. Rajabali, M. Beck, J. Haase, C. A. Lehner, W. Wegscheider, M. Failla, M. Myronov, D. R. Leadley, J. Lloyd-Hughes, P. Nataf, and J. Faist, Phys. Rev. B **101**, 075301 (2020).

[91] N. S. Mueller, Y. Okamura, B. G. Vieira, S. Juergensen, H. Lange, E. B. Barros, F. Schulz, and S. Reich, Nature (London) **583**, 780 (2020).

[92] E. Orgiu, J. George, J. A. Hutchison, E. Devaux, J. F. Dayen, B. Doudin, F. Stellacci, C. Genet, J. Schachenmayer, C. Genes, G. Pupillo, P. Samorì, and T. W. Ebbesen, Nat. Mater. **14**, 1123 (2015).

[93] M. Kiffner, J. R. Coulthard, F. Schlawin, A. Ardavan, and D. Jaksch, Phys. Rev. B **99**, 085116 (2019); New J. Phys. **21**, 073066 (2019).

[94] J. Li, L. Schamriß, and M. Eckstein, Phys. Rev. B **105**, 165121 (2022).

[95] I. V. Tokatly, D. R. Gulevich, and I. Iorsh, Phys. Rev. B **104**, L081408 (2021).

[96] X. Wang, E. Ronca, and M. A. Sentef, Phys. Rev. B **99**, 235156 (2019).

[97] O. V. Kibis, O. Kyriienko, and I. A. Shelykh, Phys. Rev. B **84**, 195413 (2011).

[98] Y. Ashida, A. İmamoğlu, and E. Demler, Phys. Rev. Lett. **126**, 153603 (2021).

[99] Y. Ashida, T. Yokota, A. İmamoğlu, and E. Demler, Phys. Rev. Res. **4**, 023194 (2022).

[100] J. Li, D. Golez, G. Mazza, A. J. Millis, A. Georges, and M. Eckstein, Phys. Rev. B **101**, 205140 (2020).

[101] A. Chiocchetta, D. Kiese, C. P. Zelle, F. Piazza, and S. Diehl, Nat. Commun. **12**, 5901 (2021).

[102] C.-R. Mann, S. A. R. Horsley, and E. Mariani, Nat. Photon. **14**, 669 (2020).

[103] C.-R. Mann, T. J. Sturges, G. Weick, W. L. Barnes, and E. Mariani, Nat. Commun. **9**, 2194 (2018).

[104] D. M. Juraschek, T. Neuman, J. Flick, and P. Narang, Phys. Rev. Res. **3**, L032046 (2021).

[105] D. Hagenmüller, J. Schachenmayer, S. Schütz, C. Genes, and G. Pupillo, Phys. Rev. Lett. **119**, 223601 (2017).

[106] D. Hagenmüller, S. Schütz, J. Schachenmayer, C. Genes, and G. Pupillo, Phys. Rev. B **97**, 205303 (2018).

[107] N. Bartolo and C. Ciuti, Phys. Rev. B **98**, 205301 (2018).

[108] I. Amelio, L. Korosec, I. Carusotto, and G. Mazza, Phys. Rev. B **104**, 235120 (2021).

[109] G. M. Andolina, F. M. D. Pellegrino, V. Giovannetti, A. H. MacDonald, and M. Polini, Phys. Rev. B **100**, 121109(R) (2019).

[110] C. A. Downing, T. J. Sturges, G. Weick, M. Stobińska, and L. Martín-Moreno, Phys. Rev. Lett. **123**, 217401 (2019).

[111] C. A. Downing and A. J. Toghill, Sci. Rep. **12**, 11630 (2022).

[112] T. Karzig, C.-E. Bardyn, N. H. Lindner, and G. Refael, Phys. Rev. X **5**, 031001 (2015).

[113] M. Knorr, J. M. Manceau, J. Mornhinweg, J. Nespolo, G. Biasiol, N. L. Tran, M. Malerba, P. Goulain, X. Lafosse, M. Jeannin, M. Stefinger, I. Carusotto, C. Lange, R. Colombelli, and R. Huber, Phys. Rev. Lett. **128**, 247401 (2022).

[114] S. Ravets, P. Knüppel, S. Faelt, O. Cotlet, M. Kroner, W. Wegscheider, and A. Imamoglu, Phys. Rev. Lett. **120**, 057401 (2018).

[115] S. Klembt, T. H. Harder, O. A. Egorov, K. Winkler, R. Ge, M. A. Bandres, M. Emmerling, L. Worschech, T. C. H. Liew, M. Segev, C. Schneider, and S. Höfling, Nature (London) **562**, 552 (2018).

[116] H. Konishi, K. Roux, V. Helson, and J.-P. Brantut, Nature (London) **596**, 509 (2021).

[117] T. Chervy, P. Knüppel, H. Abbaspour, M. Lupatini, S. Fält, W. Wegscheider, M. Kroner, and A. Imamoğlu, Phys. Rev. X **10**, 011040 (2020).

[118] B. Le Dé, C. J. Eckhardt, D. M. Kennes, and M. A. Sentef, J. Phys. Mater. **5**, 024006 (2022).

[119] G. Mazza and A. Georges, Phys. Rev. Lett. **122**, 017401 (2019).

[120] J. Román-Roche and D. Zueco, SciPost Phys. Lect. Notes 50 (2022).

[121] A. Thomas, E. Devaux, K. Nagarajan, G. Rogez, M. Seidel, F. Richard, C. Genet, M. Drillon, and T. W. Ebbesen, Nano Lett. **21**, 4365 (2021).

[122] P. Nataf and C. Ciuti, Phys. Rev. Lett. **104**, 023601 (2010).

[123] L. Garziano, A. Ridolfo, S. De Liberato, and S. Savasta, ACS Photon. **4**, 2345 (2017).

[124] I. M. Mirza, S. J. van Enk, and H. J. Kimble, J. Opt. Soc. Am. B **30**, 2640 (2013).

[125] A. Le Boité, M.-J. Hwang, H. Nha, and M. B. Plenio, Phys. Rev. A **94**, 033827 (2016).

[126] S. De Liberato, Phys. Rev. Lett. **112**, 016401 (2014).

[127] C. Cohen-Tannoudji, J. Dupont-Roc, and G. Grynberg, *Photons and Atoms* (Wiley, New York, 1989).

[128] R. Loudon, *The Quantum Theory of Light*, 3rd ed. (Oxford University Press, New York, 2000).

[129] S. Feigh, M. Clemens, R. Schuhmann, and T. Weiland, IEEE Trans. Magn. **40**, 647 (2004).

[130] J. L. Mañes, F. Guinea, and M. A. H. Vozmediano, Phys. Rev. B **75**, 155424 (2007).

[131] N. Marzari and D. Vanderbilt, Phys. Rev. B **56**, 12847 (1997).

[132] I. Souza, N. Marzari, and D. Vanderbilt, Phys. Rev. B **65**, 035109 (2001).

[133] N. Marzari, A. A. Mostofi, J. R. Yates, I. Souza, and D. Vanderbilt, Rev. Mod. Phys. **84**, 1419 (2012).

[134] G. Pizzi, V. Vitale, R. Arita, S. Blügel, F. Freimuth, G. Géranton, M. Gibertini, D. Gresch, C. Johnson, T. Koretsune *et al.*, J. Phys.: Condens. Matter **32**, 165902 (2020).

[135] L. Chirolli and J. E. Moore, Phys. Rev. Lett. **126**, 187701 (2021).

[136] M. Rymarz, S. Bosco, A. Ciani, and D. P. DiVincenzo, Phys. Rev. X **11**, 011032 (2021).

[137] A. Blais, A. L. Grimsmo, S. M. Girvin, and A. Wallraff, Rev. Mod. Phys. **93**, 025005 (2021).

[138] X. Gu, A. F. Kockum, A. Miranowicz, Y.-X. Liu, and F. Nori, Phys. Rep. **718-719**, 1 (2017).

[139] D. Roy, C. M. Wilson, and O. Firstenberg, Rev. Mod. Phys. **89**, 021001 (2017).